

## **Supporting Information**

### **Anchoring Ligand-Effect on Bright Contrast-Enhancing Property of Hollow Mn<sub>3</sub>O<sub>4</sub> Nanoparticle in T<sub>1</sub>-Weighted MRI**

Jihwan Lee,<sup>1</sup> Nitee Kumari,<sup>1</sup> Soo Min Kim,<sup>1</sup> Seonock Kim,<sup>1</sup> Ki-Wan Jeon,<sup>1</sup> Geun Ho Im,<sup>2</sup> Moon-Sun Jang,<sup>2</sup> Won Jae Lee,<sup>2</sup> Jung Hee Lee,<sup>2,\*</sup> and In Su Lee<sup>1,\*</sup>

<sup>1</sup>National Creative Research Initiative Center for Nanospace-confined Chemical Reactions (NCCR) and Department of Chemistry, Pohang University of Science and Technology (POSTECH), Gyeongbuk 790-784, Republic of Korea

<sup>2</sup>Department of Radiology, Samsung Medical Center, Sungkyunkwan University School of Medicine and Center for Molecular and Cellular Imaging, Samsung Biomedical Research Institute, Seoul 135-710, Republic of Korea

\*To whom correspondence should be addressed

E-mail: insulee97@postech.ac.kr (I. S. L.); hijunghee@skku.edu (J. H. L.)

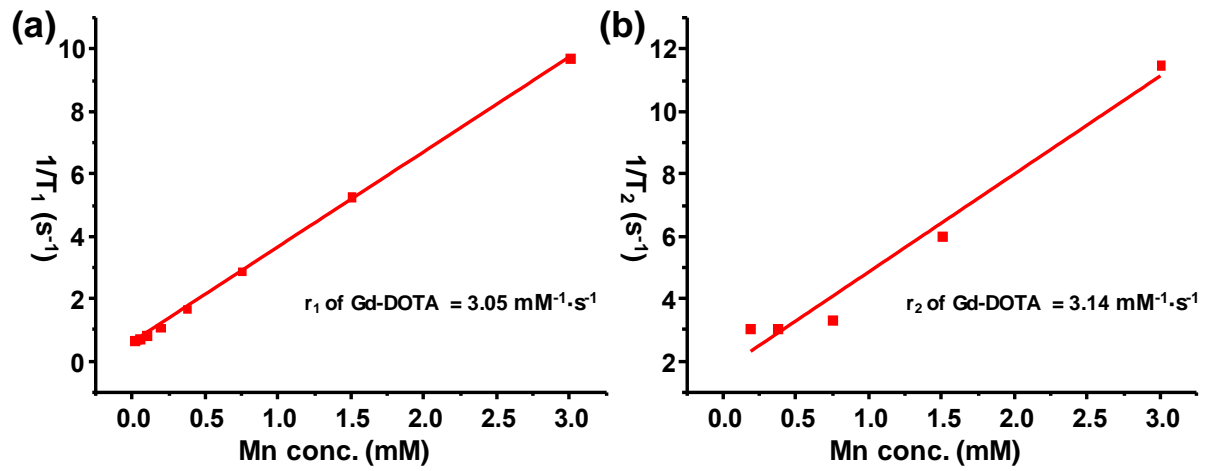


**Figure S1.** Plots of (a)  $1/T_1$  Vs [Gd] (b)  $1/T_2$  Vs [Gd] for Gd-DOTA complex.

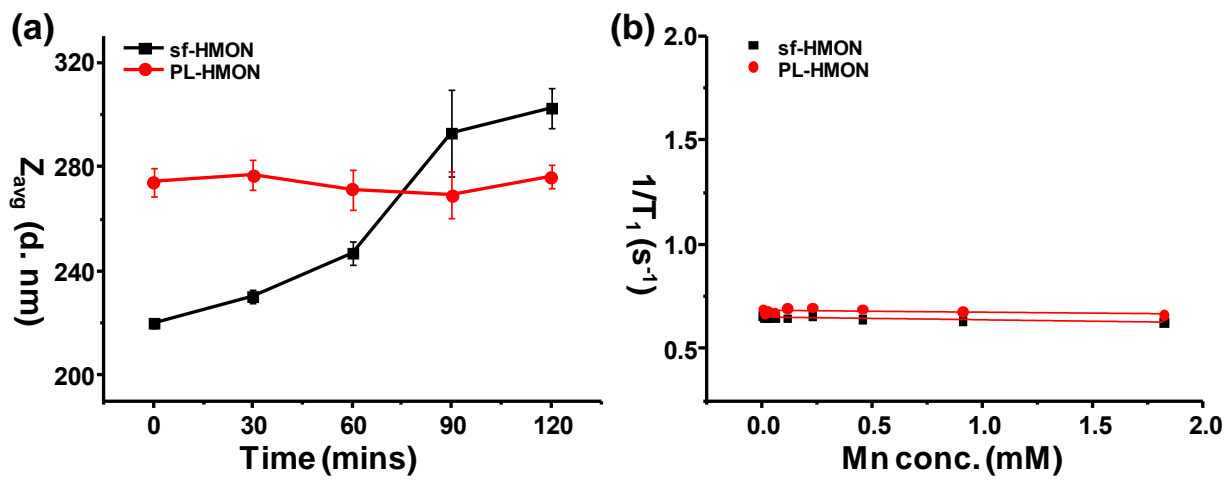


**Figure S2.** (a) Over time change in hydrodynamic diameter of **sf-HMON** and **PL-HMON** (b) Plot of  $1/T_1$  Vs [Mn] for **sf-HMON** and **PL-HMON**.

Particle	Zeta potential (mV)
<i>sf</i> -HMON	-13.42
OA-PL-HMON	-16.68
PL-HMON	-18.64
CC-PEG-HMON	-17.13
HMON@ <i>p</i> -SiO <sub>2</sub>	-44.47

**Figure S3.** Zeta potential values



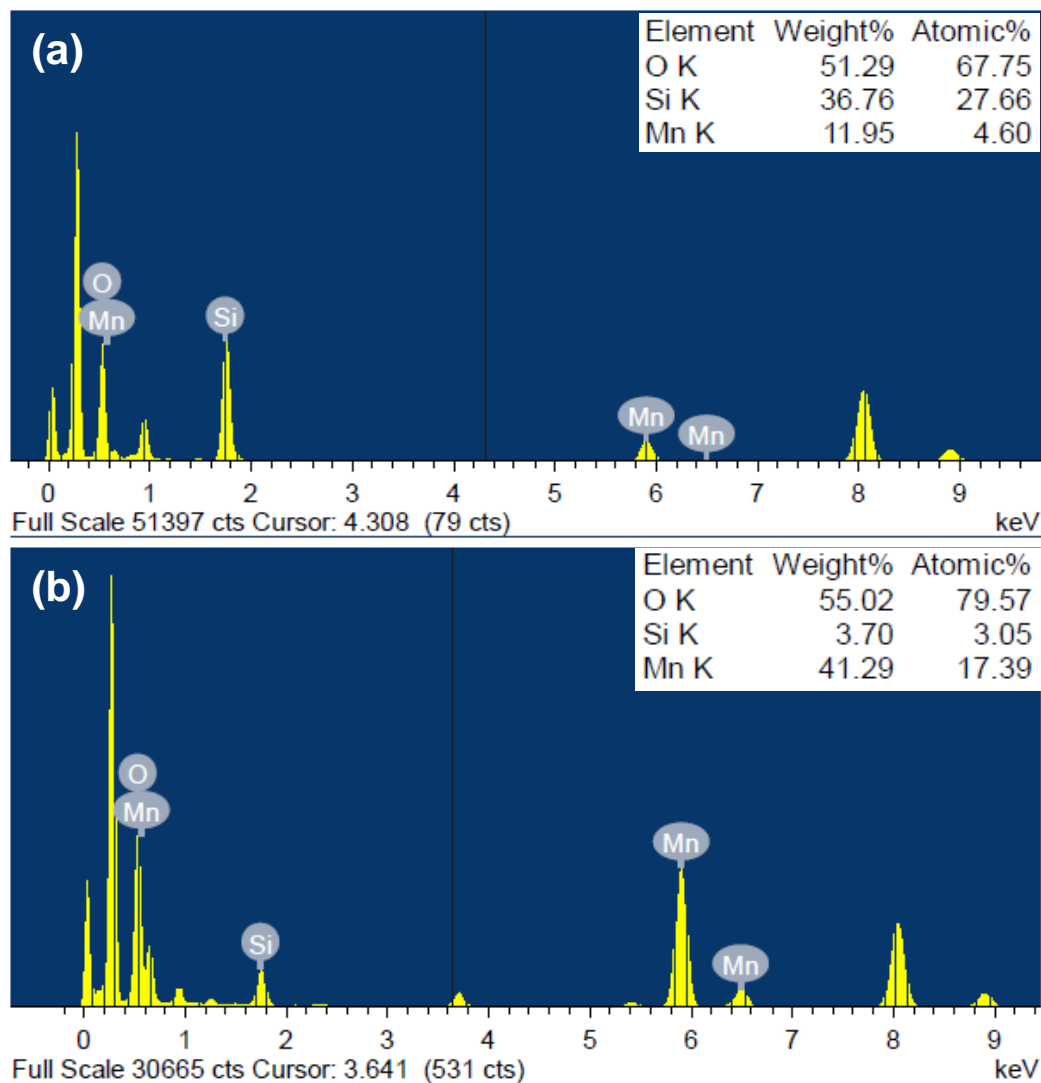


**Figure S4.** EDS spectrum of (a) HMON@*p*-SiO<sub>2</sub> (b) *sf*-HMON.

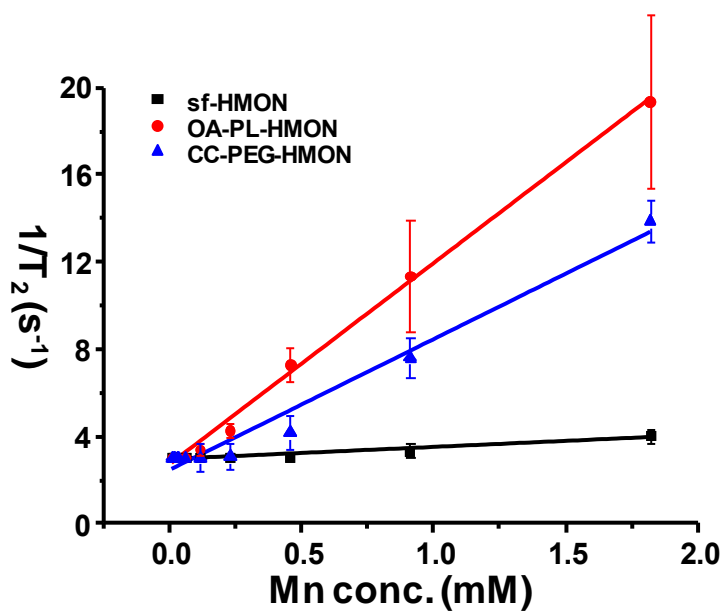


**Figure S5.** Plot of  $1/T_2$  Vs [Mn] for **sf-HMON**, **OA-PL-HMON**, and **CC-PEG-HMON**.

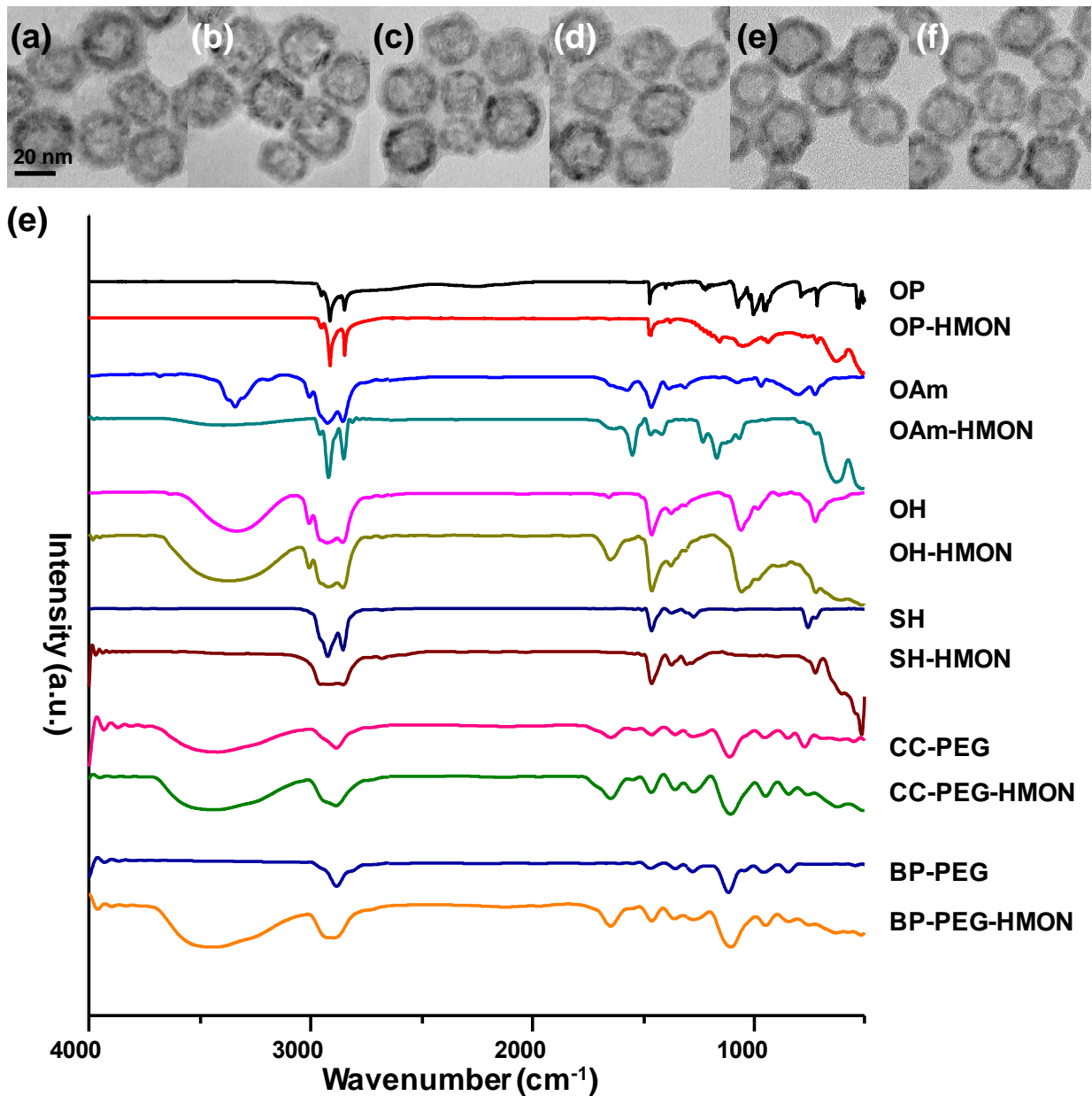


**Figure S6.** (a-f) TEM images of **OP-HMON**, **OAm-HMON**, **OH-HMON**, **SH-HMON**, **CC-PEG-HMON**, and **BP-PEG-HMON**, respectively. (e) FT-IR spectrum of Octadecylphosphonic acid, **OP-HMON**, Oleylamine, **OAm-HMON**, Oleyl alcohol, **OH-HMON**, 1-hexadecanethiol, **SH-HMON**, mPEG-Dopamine, **CC-PEG-HMON**, mPEG-BP, and **BP-PEG-HMON**.

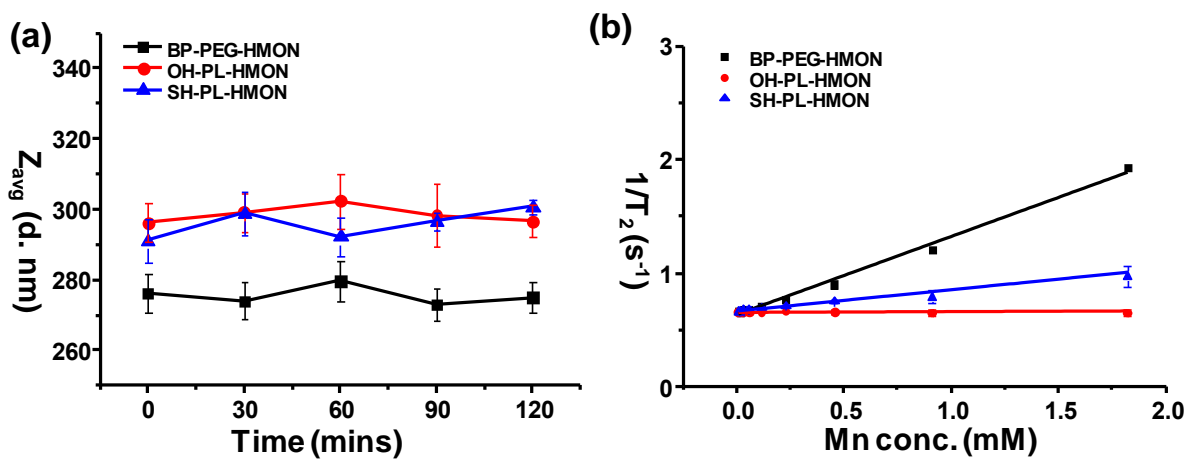


**Figure S7.** (a) Change over time in hydrodynamic diameter of **BP-PEG-HMON**, **OH-PL-HMON** and **SH-PL-HMON** (b) Plot of  $1/\tau_2$  Vs [Mn] for **BP-PEG-HMON**, **OH-PL-HMON**, and **SH-PL-HMON**.

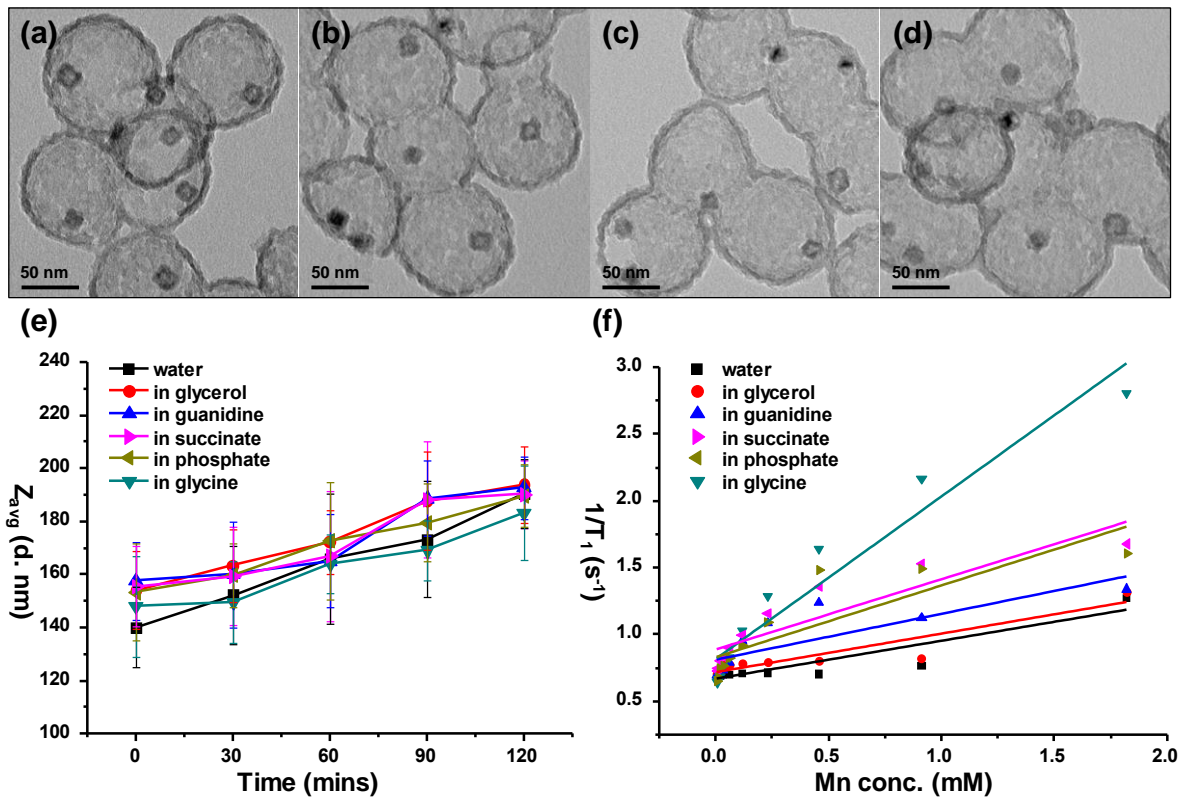


**Figure S8.** (a-d) TEM images of HMON@*h*-SiO<sub>2</sub> in guanidine, glycerol, phosphate, and glycine, respectively. (e) Change over time in hydrodynamic diameter of HMON@*h*-SiO<sub>2</sub> in water, guanidine, glycerol, succinate, phosphate, and glycine (f) Plots of  $1/T_1$  Vs [Mn] for HMON@*h*-SiO<sub>2</sub> in water (i), glycerol (ii), guanidine (iii), succinate (iv), phosphate (v) and glycine (vi)

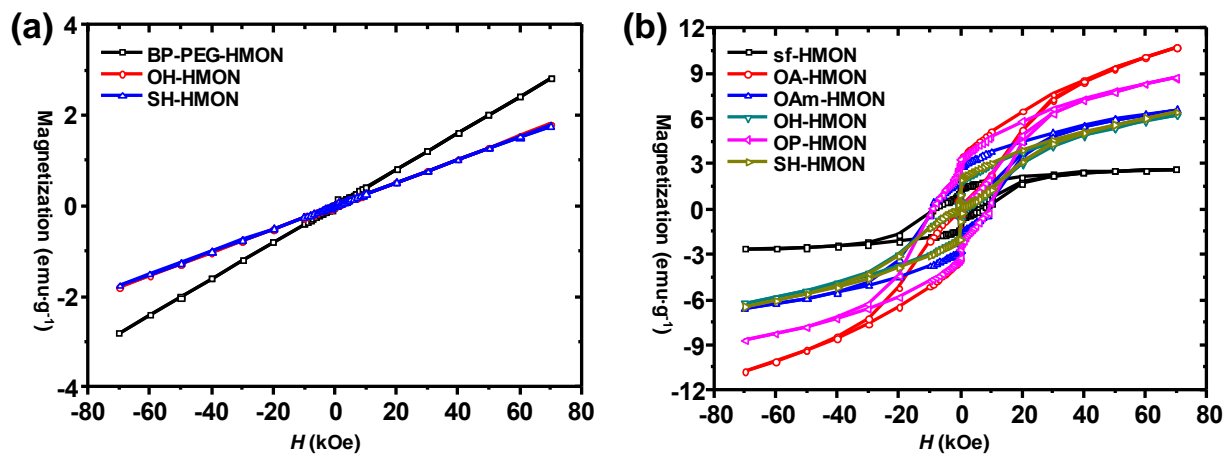


**Figure S9.** The  $M$ - $H$  curves of (a) **BP-PEG-HMON**, **OH-HMON**, and **SH-HMON** measured at 300 K and (b) **sf-HMON**, **OA-HMON**, **OAm-HMON**, **OH-HMON**, **OP-HMON**, and **SH-HMON** at 5K under an applied magnetic field from -70 to 70 kOe

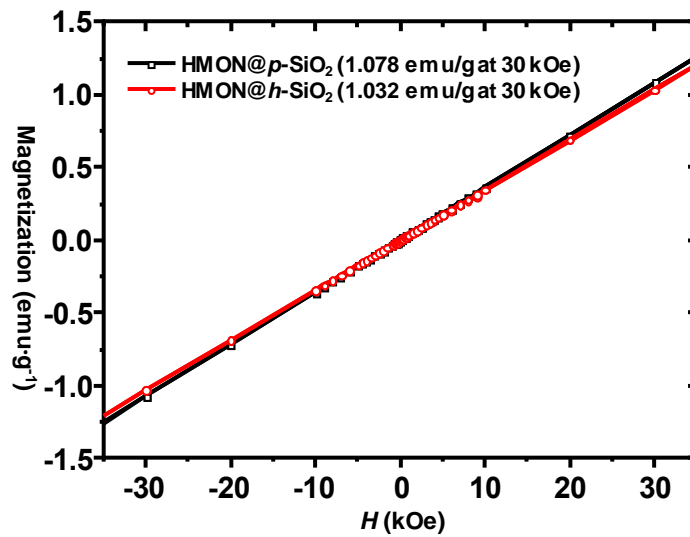


**Figure S10.** The  $M$ – $H$  curves of HMON@*p*-SiO<sub>2</sub> and HMON@*h*-SiO<sub>2</sub> measured at 300 K under an applied magnetic field from -30 to 30 kOe

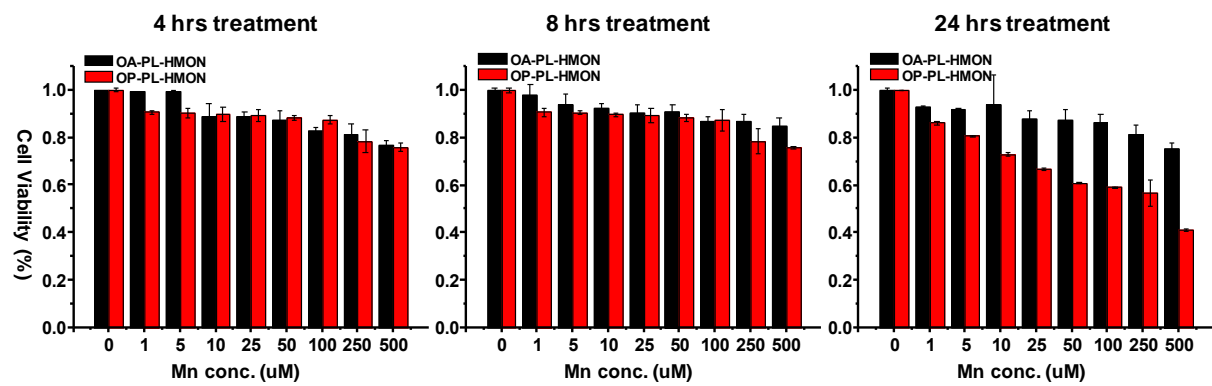


**Figure S11.** In vitro cytotoxicity of **OA-PL-HMON** and **OP-PL-HMON** for primary neuron cells.

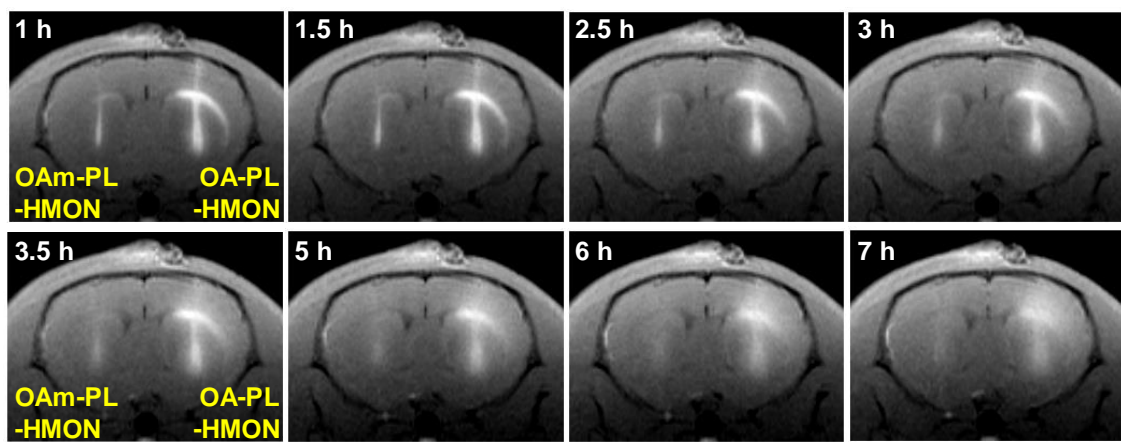


**Figure S12.** Time course of T<sub>1</sub>-weighted MR images of mouse brain injected with **OAm-PL-HMON** (left) and **OA-PL-HMON** (right).

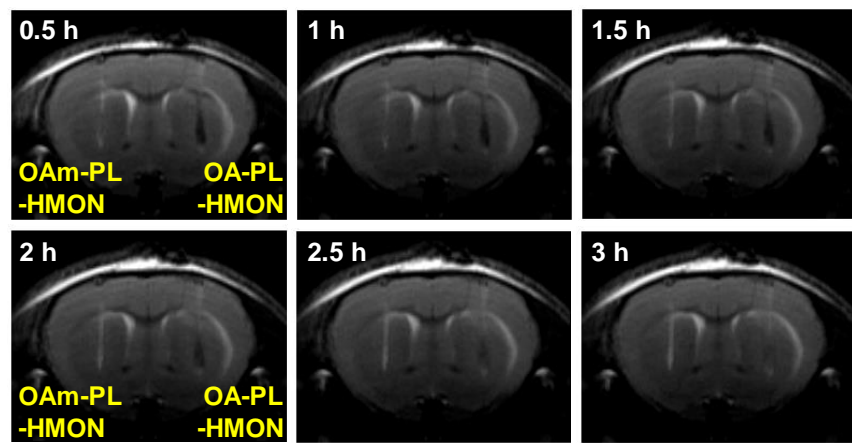


**Figure S13.** Time course of T<sub>2</sub>-weighted MR images of mouse brain injected with **OAm-PL-HMON** (left) and **OA-PL-HMON** (right).

**Table S1.** Literature reports on different strategies used to enhance the relaxivity of manganese oxide nanoparticle based contrast agents.

Material	Morphology	Av. Size (nm)	Strategy	$r_1$ (mM <sup>-1</sup> ·s <sup>-1</sup> )	$r_2$ (mM <sup>-1</sup> ·s <sup>-1</sup> )	$r_2/r_1$	Conclusion	Ref
MnO- Mn <sub>3</sub> O <sub>4</sub>	Nanocubes	9~21	Coating of manganese oxide nanocubes with small molecules	11.76 (in 0.5 T)	20.58 (in 0.5 T)	1.75	Increased surface-to-volume ratio and relative low magnetic susceptibilities of magnetic core	(24)
MnO @SiO <sub>2</sub>	Multiple/Single hollow- MON@SiO <sub>2</sub>	16	Multiple hollow MONs were encapsulated in perforated SiO <sub>2</sub> -PEO for in situ surface modification of MONs	2.58/1.23 (in 7 T)	-	-	Morphology and number of MONs encapsulated in SiO <sub>2</sub> can alter $r_1$ value	(25)
Mn <sub>3</sub> O <sub>4</sub>	Nanosphere/ Nanoplate/ Nanocube	10	Structural variation	1.31/2.06 /1.08 (in 3 T)	6.42/9.76 /9.86 (in 3 T)	4.90/4.74 /9.13	Nanoplates have largest $r_1$ value among all the nanostructures	(26)
Mn <sub>3</sub> O <sub>4</sub>	Solid/Hollow Nanospheres	20	By selective dissolution of MnO core	0.21/1.42 (in 3 T)	1.49/7.76 (in 3 T)	7.10/5.46	Hollow structures provide the facility for drug loading, water accessibility and contrast efficiency	(27)
MnO	2D-Nanoplates	8/20	Surfactant-mediated structural control	5.5/2.13 (in 7 T)	9.86/4.31 (in 7 T)	1.79/2.02	High $r_1$ value is attributed to subnanometer thickness of nanoplates	(28)
HMnO @mSiO <sub>2</sub>	Hollow nanosphere	15	HMnO is coated with mesoporous silica	0.99 (in 11.7 T)	11.02 (in 11.7 T)	11.13	Mesoporous silica allows easy access for water molecules to the magnetic core	(29)

Material	Morphology	Av. Size (nm)	Strategy	$r_1$ (mM <sup>-1</sup> ·s <sup>-1</sup> )	$r_2$ (mM <sup>-1</sup> ·s <sup>-1</sup> )	$r_2/r_1$	Conclusion	Ref
PASP-MONs	Nanospheres	10	More hydrophilic PASP was chosen over PL-PEG for surface coating	1.29 (in 7 T)	-	-	Enhanced hydrophilic by surface coating increases the water-manganese interactions	(30)
MnO @ <i>h</i> -SiO <sub>2</sub>	Nano-rattle	16	MnO is coated with permeable silica nanoshell perforated by the PEO chains	1.17 (in 7 T)	30.73 (in 7 T)	26.26	Hollow SiO <sub>2</sub> with PEO chains improves accessibility of water molecules to the MnO core	(31)
MnO @ mSiO <sub>2</sub>	Core-Shell nanosphere	23	MnO core with variable shapes are coated with non-porous and mesoporous SiO <sub>2</sub>	0.17/0.92 /0.16/0.2 (in 0.47 T)	5.18/7.48 /1.60/1.7 8 (in 0.47 T)	30.47/8.1 3/10/8.9	The high $r_1$ relaxivity was attributed to the worm like anochannels in SiO <sub>2</sub> for facilitated water exchanging rate	(32)
MnO-TETT-FA	Nanospheres	16	Surface coating with TETT and folic acid enhances biocompatibility and specific targeting ability of MnO	4.84 (in 7 T)	-	-	Thickness of silane layer shortens the distance between external Mn ion and water protons	(33)
HSA-MnO	Nanospheres	20	superior ligand binding affinity of HSA conferred extra stability to the particles	1.97 (in 7 T)	-	-	Compact and hydrophilic coating allows more efficient water-metal interaction	(34)

※ The relaxivity values measured under different magnetic field strength are not comparable